



Effect of multilayer graphene/nano-Fe₂O₃ composite additions on dry sliding wear behavior of titanium matrix composites

Huang Xie¹ · Yun-xue Jin^{1,2} · Mu-ye Niu^{1,2} · Ji-heng Wang^{1,2}

Received: 25 June 2019 / Revised: 15 November 2019 / Accepted: 17 November 2019 / Published online: 30 August 2020
© China Iron and Steel Research Institute Group 2020

Abstract

The wear tests of titanium matrix composites (TMCs) at the loads of 50, 100, 120, and 150 N were carried out with an MMW-1 vertical universal friction and wear tester to study the addition of multilayer graphene (MLG)/nano-Fe₂O₃ composites (0, 0.1, 0.2, 0.3, 0.4, and 0.5 g) on the dry sliding wear behavior of TMCs. TMCs presented a marked variation in wear loss as a function of the amount of MLG/Fe₂O₃ addition, and a significant decrease in the friction coefficient was obtained, reducing this parameter up to 50%. With the rise and fall of wear loss, TMCs underwent a transition from severe wear to mild wear. These phenomena were attributed to the existence of a protective lubricating film, which prevented the surface from coming in direct contact, and the lubricating film was 15–20 μm thick and made up of MLG/Fe₂O₃ (1:2) nanocomposites. Its structure was speculated to be similar to a rolling wood.

Keywords Titanium matrix composite · Graphene · Nanomaterial · Lubricating film · Wear behavior

1 Introduction

Graphene, a two-dimensional material discovered in 2004, has been investigated extensively in the recent decade and demonstrates great potential for a wide range of applications [1–4]. Multilayer graphene (MLG), a derivative of graphene, possesses similar properties to graphene, such as super charge carrier mobility, high fracture strength, high Young's modulus, and extreme thermal conductivity [5–7]. Therein, its tribological properties had been investigated on numerous research works [8–14]. Because of having a high Mohs hardness of 5.5, Fe₂O₃ is usually considered with a good load bearing capacity, which has been reported elsewhere [15–17]. Iwabuchi et al. [18] investigated the effect of Fe₂O₃ particles on the severe–mild wear transition of a sliding steel interface, and it was confirmed that this transition occurred

when a compacted oxide layer was formed. The formation of load bearing Fe₂O₃-containing tribolayers might be a prerequisite for the wear reduction.

Zhou et al. [19] investigated the additions of MLG/Fe₂O₃ (with mass proportions of 2:1, 1:1, and 1:2) nanocomposite on TC11 alloy, in order to improve the tribological properties, and results showed that MLG/Fe₂O₃ nanocomposite (1:2) drastically improved the wear resistance of TC11 alloy. Therefore, MLG/Fe₂O₃ (1:2) nanocomposite was chosen as additive on titanium matrix composites (TMCs) in this paper. TMCs have been widely investigated due to their superior properties, and with the development of TMCs, according to the practical application of various requirements, the study of the wear resistance for TMCs becomes more and more important. However, the wear test, reported by Zhou et al. [19], was conducted with a single load and did not explore how MLG/Fe₂O₃ nanocomposite (1:2) influenced the wear mechanism deeply. Based on these facts, sliding wear tests of TMCs against W6Mo5Cr4V2 high-speed steel at various loads, including 50, 100, 120, and 150 N, were performed, with the addition of MLG/Fe₂O₃ (1:2) nanocomposite on the sliding interface. The worn surfaces and subsurfaces were systematically characterized. Further, the effects of nanomaterial addition amount on the wear behavior were explored.

✉ Yun-xue Jin
jinyunxue@126.com

¹ School of Material Science and Engineering, Jiangsu University of Science and Technology, Zhenjiang 212003, Jiangsu, China

² National Demonstration Center for Experimental Materials Science and Engineering Education (Jiangsu University of Science and Technology), Zhenjiang 212003, Jiangsu, China

2 Experimental details

2.1 Material preparation

MLG/Fe₂O₃ (1:2) nanocomposite was prepared by a liquid-phase exfoliation method. The details were described as follows (Fig. 1): Firstly, a magnetic stirring apparatus was used to disperse the expanded graphite and Fe₂O₃ nanoparticles for 1 h. Then, an ultrasonic cell disruptor was applied to exfoliate the uniform mixture with the following details: 2 h for operating time, 25 s for ultrasonic time, 5 s for interval time, 30 min for stewing, 20 mm for shift lever diameter, and 540 W for the power. Subsequently, the remaining turbid liquid was centrifugally separated under a high velocity of 8000 r/min for 10 min. After that, the precipitate was washed with ethanol and dried at 343 K in a vacuum drying oven for 24 h. Finally, MLG/Fe₂O₃ nanocomposite (1:2) was obtained.

For wear test, TMCs and W6Mo5Cr4V2Co5 high-speed steel (American band: M35) were selected as pin and disk materials, respectively. Their chemical compositions are given in Table 1. Ti6Al4V bar (ϕ 10 mm), the titanium sponge (purity 99.6%), and B₄C powder (purity 99%) were chosen as raw materials for (TiC + TiB)/Ti6Al4V in situ composites and melted in a magnetron tungsten arc furnace. In order to ensure the uniformity of the composition of the sample, the preparation for each sample was repeated three times. (TiC + TiB) reinforcements with a theoretical volume fraction of 5% were obtained. Then, TMCs were machined into cylindrical pins with diameters of 5 mm and heights of 15 mm. M35 steel was machined into counterpart disks with diameters of 52 mm and thicknesses of 10 mm. After quenching at 1473.15 K for 20 min, then oil cooling, and tempering at 823.15 K for 2 h for three times, the hardness of the disks was adjusted to 64–66 HRC.

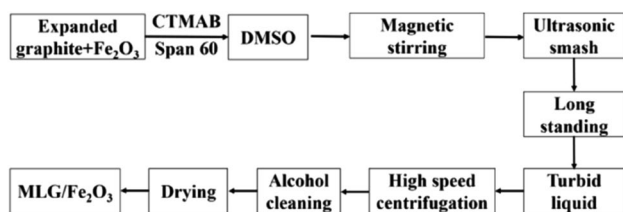


Fig. 1 Preparation process of MLG/Fe₂O₃ composites

2.2 Wear tests

Dry sliding wear tests of TMCs against M35 steel with the addition of MLG/Fe₂O₃ (1:2) nanocomposites were performed in air at room temperature using an MMW tribometer with a pin-on-disk contact geometry. Foam plastic and adhesive tape were adhered onto the center and periphery of the disk, respectively, to prevent the aggregation and spillover of additives as shown in Fig. 2. The normal loads during the wear tests were 50, 100, 120, and 150 N at a speed of 100 r/min (or 0.33 m/s). The sliding test durations were 5000 cycles or 990 m, and the amounts of adding nanocomposites were 0.1, 0.2, 0.3, 0.4, and 0.5 g, respectively. For comparison, the dry sliding wear test without any additive was also performed. Prior to each sliding, the pins and disks were initially cleaned by sonication in acetone and then in isopropanol alcohol to remove any organic contaminants that may have been left from the machining and polishing operations performed during sample preparation. An electronic balance with an accuracy of 10⁻⁴ g was used to measure the wear loss of the pins before and after tests.

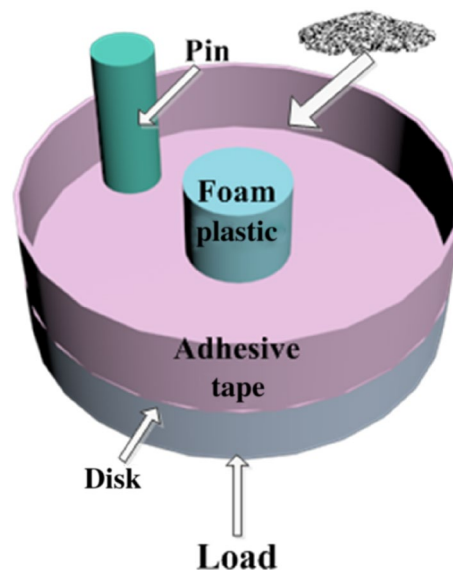


Fig. 2 Schematic diagram of dry sliding wear test setup

Table 1 Chemical compositions of TMCs and M35 steel (wt.%)

Material	C	Al	Fe	Mn	Mo	V	Ti	Cr	Co	W
TMCs		3.19	0.06	0.354	0.105	2.85	Balance			
M35	0.627		Balance	0.305	5.00	2.16		3.94	5.26	5.73

2.3 Microscopic analysis

A JEM-2100F high-resolution transmission electron microscope (TEM) and a D/Max-2500/pc type X-ray diffractometer (XRD) with Cu K α radiation were applied to characterize MLG/Fe₂O₃ nanocomposite samples. Phase constitutions of

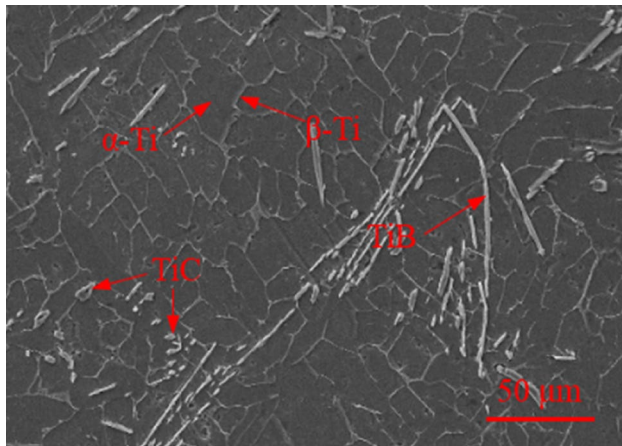


Fig. 3 Microstructure of TMCs

the worn surfaces were measured on an X-ray diffractometer and a DXR laser Raman spectrometer (Raman). A JSM-7001F scanning electron microscope (SEM) and an Inca Energy 350 energy dispersion spectrometer (EDS) were utilized for the measurement of the microstructures and compositions of the worn surfaces and subsurfaces. The roughness of the worn surfaces was measured using an OLS4000 Olympus laser confocal scanning microscope.

3 Results and analysis

3.1 Microstructure characterization

Figure 3 shows the microstructure of TMCs. It can be seen that TMCs were composed of α -Ti phase, β -Ti phase, TiB phase, and TiC phase. The matrix exhibited typical $\alpha + \beta$ dual-phase microstructure (whisker-like TiB and granular TiC).

Figure 4 shows TEM images of MLG (with an SEM inset), Fe₂O₃ and MLG/Fe₂O₃ nanocomposites. From Fig. 4a, the prepared MLG was observed to be a nanometer-thick lamellar structure, which was almost transparent. In

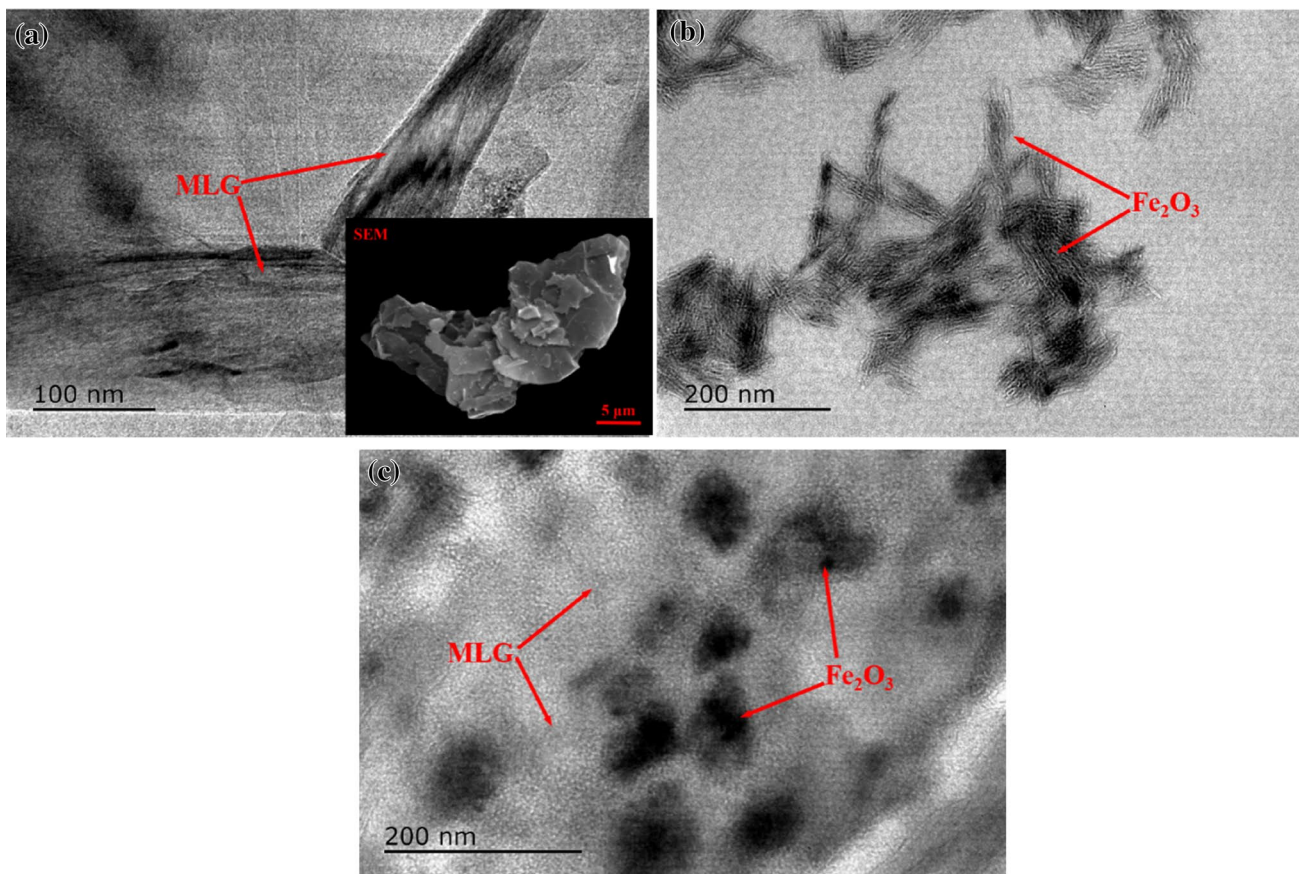


Fig. 4 TEM images of MLG (a), Fe₂O₃ (b) and MLG/Fe₂O₃ nanocomposite (c). Inset in a is SEM image of MLG

Fig. 4b, Fe_2O_3 was noticeably agglomerated, and its form was difficult to distinguish. However, in MLG/ Fe_2O_3 nanocomposite, shown in Fig. 4c, the degree of agglomeration of Fe_2O_3 nanoparticles was drastically decreased. Instead, the spindle-shaped Fe_2O_3 particles were randomly distributed on the surface of MLG. Clearly, Fe_2O_3 was successfully composited with MLG.

3.2 Wear loss

Figure 5 illustrates the wear loss of TMCs as a function of MLG/ Fe_2O_3 addition amount under different loads, and it is found that TMCs presented a marked variation in wear loss as a function of MLG/ Fe_2O_3 addition. In general, different varying trends of wear loss were demonstrated with an increase in MLG/ Fe_2O_3 addition under different loads. At the load of 50 N, the wear loss varied in two stages, corresponding to MLG/ Fe_2O_3 additions of 0.1 g and 0.2–0.5 g, respectively. Less MLG/ Fe_2O_3 nanocomposites caused an obvious increase in the wear loss, but with more MLG/ Fe_2O_3 nanocomposites addition, the wear loss reached an extremely low value. At the load of 100 N, when MLG/ Fe_2O_3 addition increased from 0.1 to 0.5 g, the wear loss decreased to a lowest value at first, then approximately maintained around zero with MLG/ Fe_2O_3 addition ranging from 0.2 to 0.4 g, and then eventually increased at 0.5 g. As for 120 N, when MLG/ Fe_2O_3 addition increased from 0.1 to 0.3 g, the wear loss slightly increased to reach a peak at 0.3 g and then substantially decreased to a lowest point at 0.5 g. In order to further explore the influence of MLG/ Fe_2O_3 addition, the test with an MLG/ Fe_2O_3 addition of 0.6 g at 120 N was conducted, and the wear loss rapidly increased beyond 0.5 g. At the load of 150 N, comparing with that at the load of 120 N, almost the same wear loss varying trend was showed with MLG/

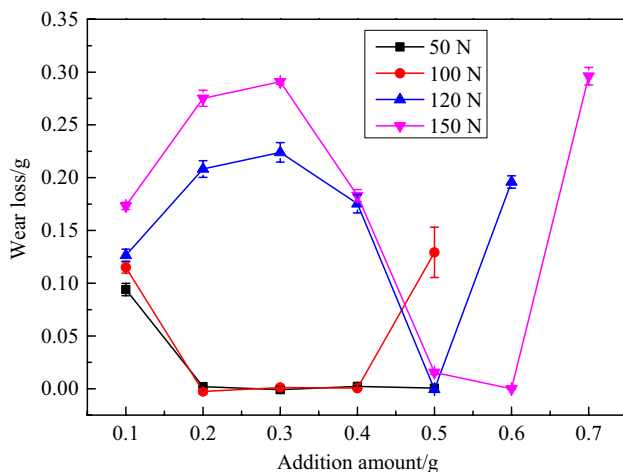


Fig. 5 Wear loss of TMCs as a function of MLG/ Fe_2O_3 addition under different loads

Fe_2O_3 addition ranging from 0.1 to 0.5 g. Similarly, complementary experiments were conducted with MLG/ Fe_2O_3 addition of 0.6–0.7 g at 150 N, and the wear loss remained low at 0.6 g but rapidly increased at 0.7 g. Therefore, there appeared to be a critical point of MLG/ Fe_2O_3 addition on the wear loss versus MLG/ Fe_2O_3 addition curves under different loads.

Friction coefficient (μ) of TMCs against M35 steel as a function of MLG/ Fe_2O_3 addition under different loads is presented in Fig. 6. It can be observed that the friction coefficient varied with the load and MLG/ Fe_2O_3 addition. Obviously, the friction coefficient exhibited a similar varying trend as compared to the wear loss (Fig. 5). At 50 N, the friction coefficient was firstly increased and reached a friction coefficient value of 0.385. However, with a further increase in MLG/ Fe_2O_3 addition from 0.2 to 0.5 g, the friction coefficient decreased to a certain platform with a range of 0.126–0.187. At the load of 100 N, the friction coefficient maintained at low stable values with MLG/ Fe_2O_3 addition range of 0.2–0.4 g, and the coefficient increased with MLG/ Fe_2O_3 addition of either 0.1 or 0.5 g. As the load varied between 120 and 150 N, the critical MLG/ Fe_2O_3 addition value increased to 0.5 g and (0.5–0.6) g, respectively.

3.3 XRD analysis of worn surfaces

XRD patterns and Raman spectra are shown in Fig. 7. From Fig. 7a, at the load of 50 N, with MLG/ Fe_2O_3 addition of 0.1 g, only Ti, TiC, and TiB were detected on the worn surface. However, MLG was detected in XRD patterns with the

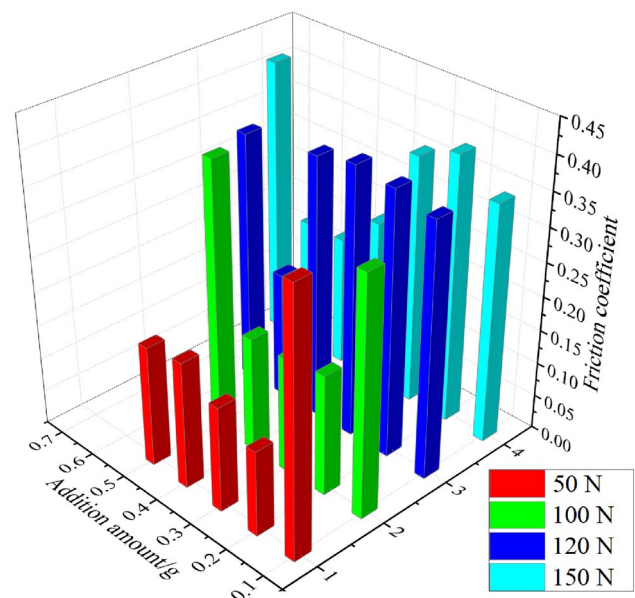


Fig. 6 Friction coefficient of TMCs as a function of MLG/ Fe_2O_3 addition under different loads

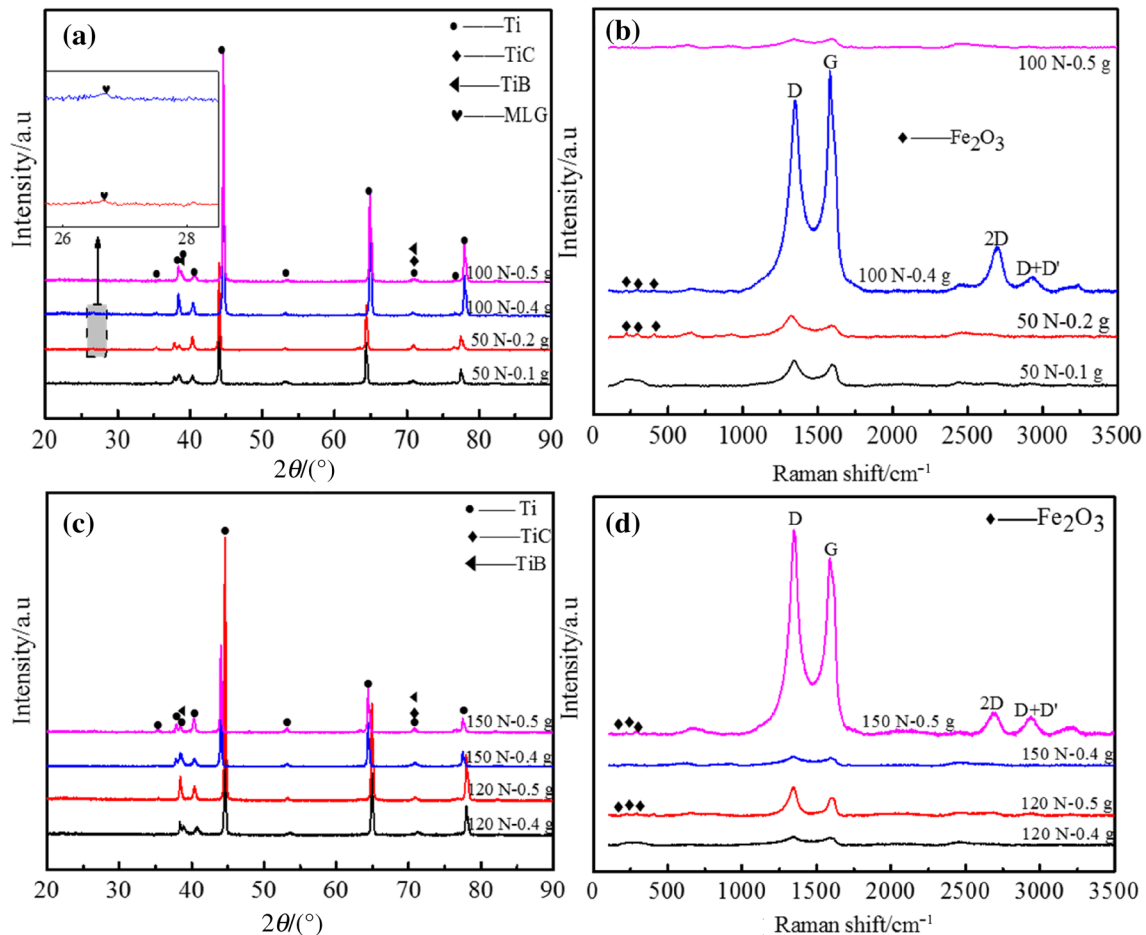


Fig. 7 XRD patterns (a, c) and Raman spectra (b, d) of worn surfaces of TMCs with MLG/Fe₂O₃ (1:2) nanocomposites at loads of 50 and 100 N (a, b) as well as 120 and 150 N (c, d)

addition of 0.2 g of MLG/Fe₂O₃ (1:2) nanocomposites, but no Fe₂O₃ was observed in XRD pattern. Whether Fe₂O₃ was detected on the worn surface could be verified by the Raman spectrums, as shown in Fig. 7b. It is obvious that the peaks of Fe₂O₃ emerged except for the ones of MLG, indicating that there was Fe₂O₃ on worn surfaces, while minor amount of Fe₂O₃ could be hardly identified by XRD. At the load of 100 N, MLG appeared with 0.4 g MLG/Fe₂O₃ addition (but not observed with 0.5 g addition), which could also be verified by the Raman spectrum, as shown in Fig. 7b. As shown in Fig. 7c, d, both MLG and Fe₂O₃ emerged on the worn surfaces with 0.5 g addition of MLG/Fe₂O₃ (1:2) nanocomposites at the load of both 120 and 150 N. The absence of MLG and Fe₂O₃ in XRD patterns resulted from either a tiny quantity or nonexistence. Whether or not MLG and Fe₂O₃ were actually present was determined by Raman spectra, shown in Fig. 7d. It is worth mentioning that three main characteristic peaks, D mode (~1350 cm⁻¹), G mode (~1580 cm⁻¹), and 2D mode (~2700 cm⁻¹), were adopted to examine the existence of MLG [20]. And D+D' (at ~2940 cm⁻¹) was

activated by defects in the graphene layers. This finding supports the fact that sliding interfaces produce defected graphene. Therefore, it is clear that when both MLG and Fe₂O₃ emerged on the worn surfaces, the wear loss reached an extremely low value. On the other hand, when MLG/Fe₂O₃ addition amount was higher than critical value, both of MLG and Fe₂O₃ disappeared.

3.4 Morphology of worn surfaces

The morphologies of worn surfaces with different amounts of MLG/Fe₂O₃ (1:2) nanocomposites addition are shown in Fig. 8. At the load of 50 N, with 0.1 g MLG/Fe₂O₃ addition, the worn surface of TMCs presented typical characteristics of adhesive and abrasive wear, including adhesive traces, furrows, and severe delaminated regions. Additionally, a small amount of wear debris was remained on the worn surfaces. Conversely, the worn surface with 0.2 g addition amount was found smoother, and furrows were narrower and shallower than those of 0.1 g MLG/Fe₂O₃ one. It is

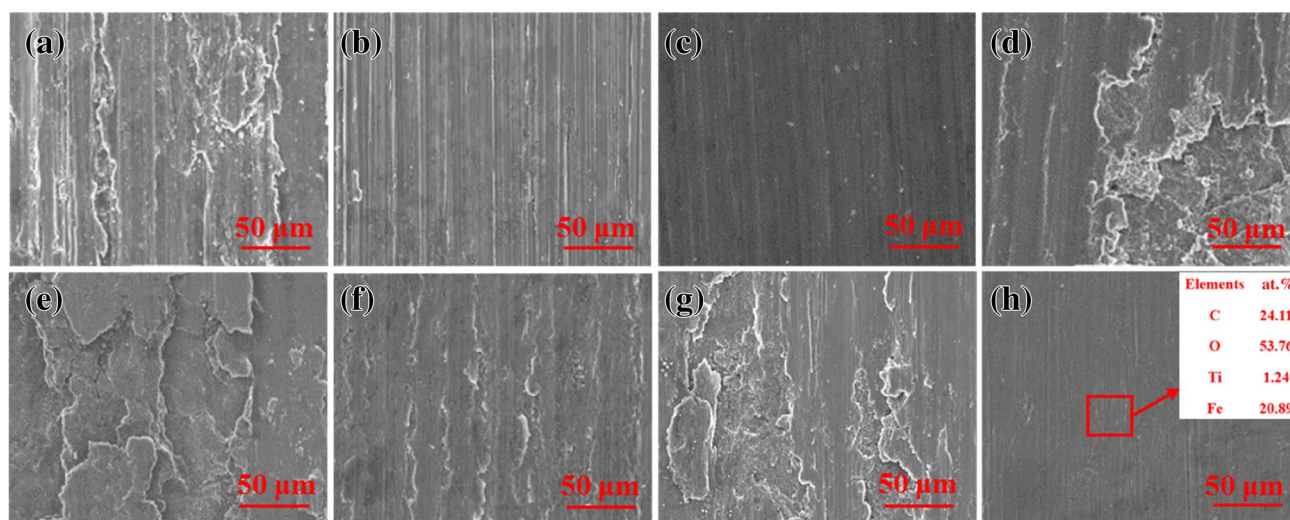


Fig. 8 SEM morphologies of worn surfaces of TMCs under various conditions. **a** 50 N–0.1 g; **b** 50 N–0.2 g; **c** 100 N–0.4 g; **d** 100 N–0.5 g; **e** 120 N–0.4 g; **f** 120 N–0.5 g; **g** 150 N–0.4 g; **h** 150 N–0.5 g

clear that the addition of MLG/Fe₂O₃ (1:2) nanocomposites improved the wear resistance effectively. As for 100 N, a well-protected worn surface appeared with 0.4 g MLG/Fe₂O₃ addition, while severe plastic tearing was shown on the worn surface with 0.5 g MLG/Fe₂O₃ addition, whose variation implied that TMCs might have undergone a severe wear owing to the excessive MLG/Fe₂O₃ addition amount. A similar transition of the morphologies of TMCs worn surfaces was shown at the load of both 120 and 150 N. When MLG/Fe₂O₃ addition amount was 0.4 g (Fig. 8e, g), the worn surfaces were far severer than those with 0.5 g addition (Fig. 8f, h), whose worn surfaces were smoother and neater than those with 0.4 g addition. A large amount of C, O, and Fe elements were detected on the worn surfaces as shown in EDS analysis (Fig. 8h), which indicates that MLG/Fe₂O₃ (1:2) nanocomposites remained on the worn surface, inducing a good protection on the surface and further resulting in the extremely low value of the wear loss.

3.5 Cross-sectional morphology of worn surfaces and subsurfaces

The cross-sectional morphologies of worn surfaces and subsurface with different amounts of MLG/Fe₂O₃ (1:2) nanocomposites addition are shown in Fig. 9. At the load of 50 N, a sporadic, discontinuous tribolayer was formed on the worn surfaces with 0.1 g MLG/Fe₂O₃ addition. Underneath the tribolayer, plastic deformation took place in the subsurface regions, but it was not very intensive (Fig. 9a). However, within 50 N–0.2 g sample, a ceramic-like tribolayer appeared and there was no plastically deformed layer underneath the worn surface, as shown in Fig. 9b, corresponding to the extremely low value of the wear loss in

Fig. 5. As for the load of 100 N, the morphology of worn surface and subsurface with 0.4 g MLG/Fe₂O₃ addition, as shown in Fig. 9c, was similar to that of 50 N–0.2 g sample. When MLG/Fe₂O₃ addition increased to 0.5 g, the plastically deformed tribolayer appeared on the worn surface and at the subsurface, respectively (Fig. 9d). However, the tribolayer was thicker and more irregular. As for the cases of both 120 and 150 N, with 0.4 g addition, the tribolayer was characterized by cracks, discontinuity, and deformed regions, as shown in Fig. 9e, g. However, as the amount of MLG/Fe₂O₃ addition reached the critical value (0.5 g), the plastically deformed region thoroughly vanished, as observed in Fig. 9f, h.

4 Discussion

4.1 Formation and characteristics of lubricating film

During the wear process, a lubricating film was formed on both the pin and the disk, which accounted for the appearing excellent tribological properties. The microstructures of both the pin and the disk were investigated, and line profile measurements and Raman tests were conducted to characterize the lubricating film. The results show that the lubricating film formed on the disk was found more complete than that formed on the pin, as shown in Fig. 10. Along the sliding track, a thin, dense, silvery white lubricating film was formed (Fig. 10a). The destruction of the lubricating film initiated from the edges and expanded to the central region because the lubricating film suffered higher Hertz pressure effects on the edges than the central region. Thus,

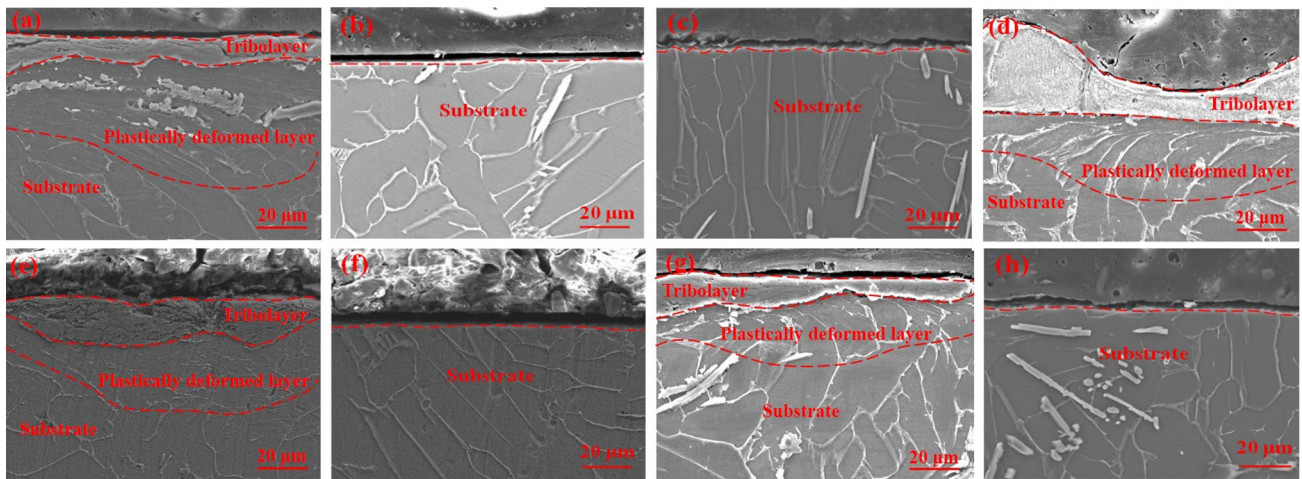


Fig. 9 Cross-sectional morphologies of TMCs worn surfaces under various conditions. **a** 50 N–0.1 g; **b** 50 N–0.2 g; **c** 100 N–0.4 g; **d** 100 N–0.5 g; **e** 120 N–0.4 g; **f** 120 N–0.5 g; **g** 150 N–0.4 g; **h** 150 N–0.5 g

the lubricating film on the edges was readily destroyed and gradually resulted in the sandwich-like morphology (Fig. 10b, c). As the sliding distance surpassed a critical point, the lubricating film was completely consumed.

A further investigation was taken to characterize the lubricating film, as shown in Fig. 11. Figure 11a shows a 3D profilometer image of the lubricating film with MLG/Fe₂O₃ addition of 0.3 g at the load of 50 N, indicating that the height of the lubricating film is 15–20 μm. Whether the lubricating film was made up of MLG/Fe₂O₃ (1:2) nanocomposites could be verified by the Raman spectrums, as shown in Fig. 11b, and it is obvious that Fe₂O₃ peaks were detected while those of MLG were not, indicating that the lubricating film was composed of MLG/Fe₂O₃ (1:2) nanocomposites. It is also worth noting that D + D' (at ~2940 cm⁻¹) appeared on both curves, supporting the fact that defected graphene was produced on the sliding interfaces after a certain degree of sliding distance.

Generally, the formation of the lubricating film was affected by numerous factors, such as the environment temperature, normal load, sliding speed, additives, and mechanical, thermal and chemical properties of the materials. In our present work, the normal load and the amount of additives were the two important factors, which influenced the formation of the lubricating film directly. At the lower load (50 N), as the amount of MLG/Fe₂O₃ addition surpassed 0.1 g, the lubricating film started to form, and film formation remained until MLG/Fe₂O₃ addition reached 0.5 g. However, at the higher load (100, 120 and 150 N), there appeared to be a critical range of amount of MLG/Fe₂O₃ addition, and while the amount of addition fell below or above the critical value, the lubricating film could not form. It is presumed that the formation of the lubricating film involved physical or

chemical reactions, and only while a critical condition was satisfied, the lubricating film could exist. Below the critical value of MLG/Fe₂O₃ amount, there were not enough MLG/Fe₂O₃ (1:2) nanocomposites to form the lubricating film. Above the critical value of the additive amount, the film formation was likely to be limited by free energy, which was dependent on an increase in temperature [17]. During sliding at room temperature, the ambient temperature is mainly dependent on the frictional heat (q).

$$q = \mu P v \quad (1)$$

where P is the applied load and v is the sliding velocity [21]. In the present work, since the sliding velocity was fixed, the friction coefficient was almost identical under a certain load, which resulted in the similar temperature and free energy. Therefore, when the additive amount was above the critical value, a favorable free energy was absent, discouraging the formation of a lubricating film.

4.2 Wear mechanism

Schematic illustration of the wear mechanism is given in Fig. 12. In the present work, the mechanism was mainly related to the lubricating film. As shown in Fig. 12a, during the wear sliding process, a lubricating film was formed due to the addition of MLG/Fe₂O₃ (1:2) nanocomposites, rendering the excellent anti-friction and wear-resistant properties of the surfaces of both the pin and the disk. Moreover, there was absolutely no plastic deformation at this time (Fig. 12b), and the film showed an excellent protection owing to MLG/Fe₂O₃ (1:2) nanocomposites, which resulted in the extremely low value of

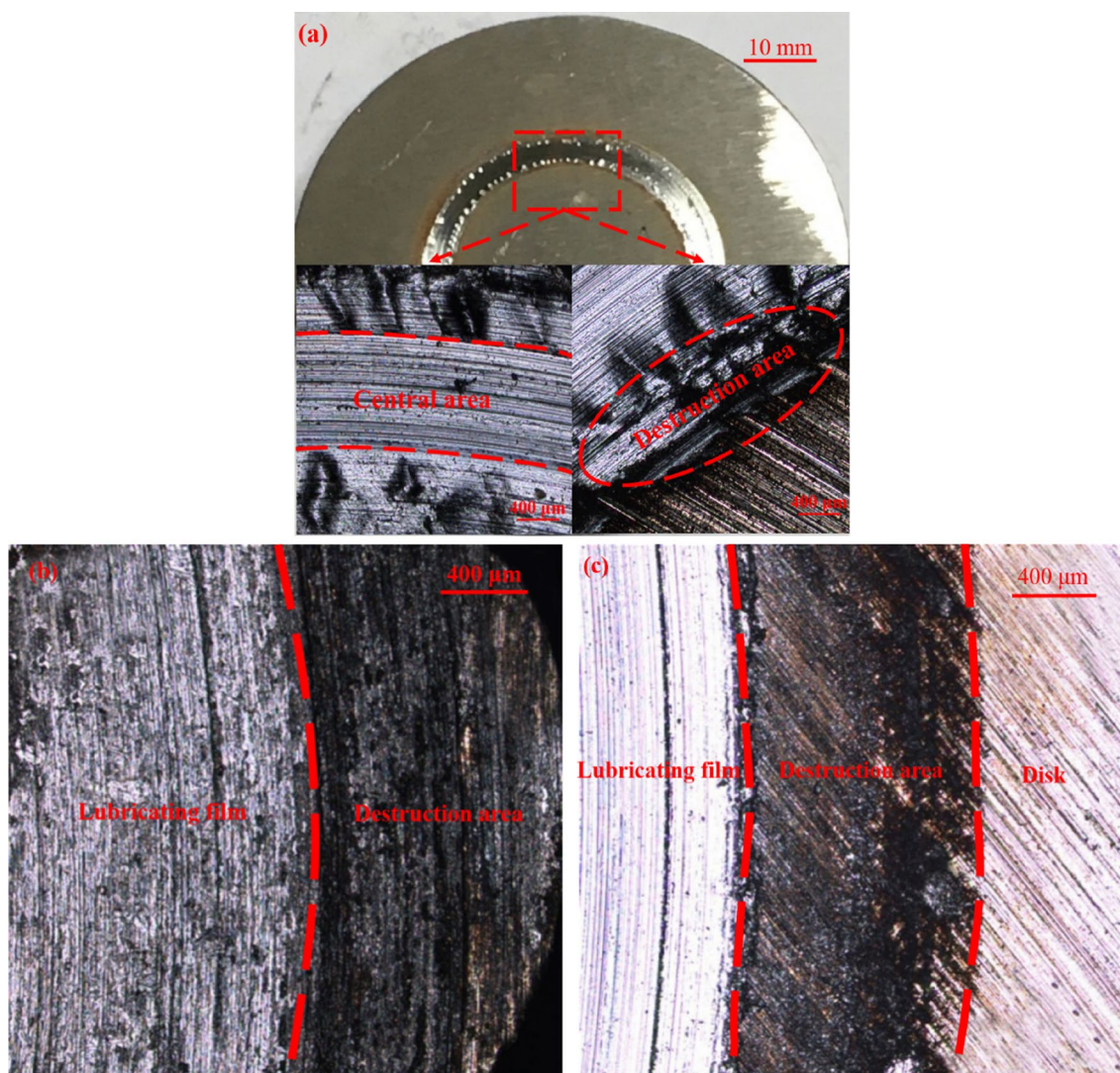


Fig. 10 Macroscopic image of lubricating film (a), pin (b) and disk (c)

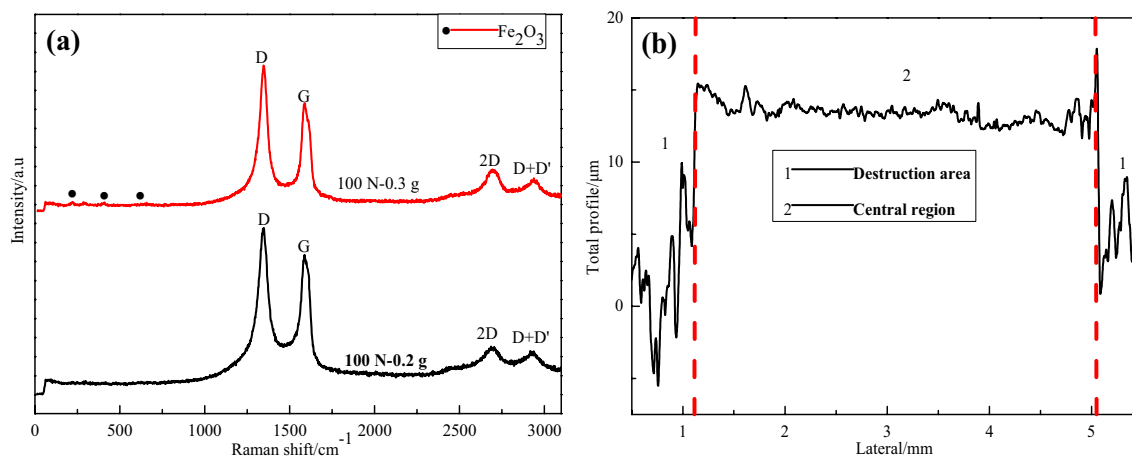


Fig. 11 Characteristics of lubricating film. **a** Raman spectra of lubricating film with different amounts of MLG/Fe₂O₃ addition at a load of 100 N; **b** 3D profilometer image

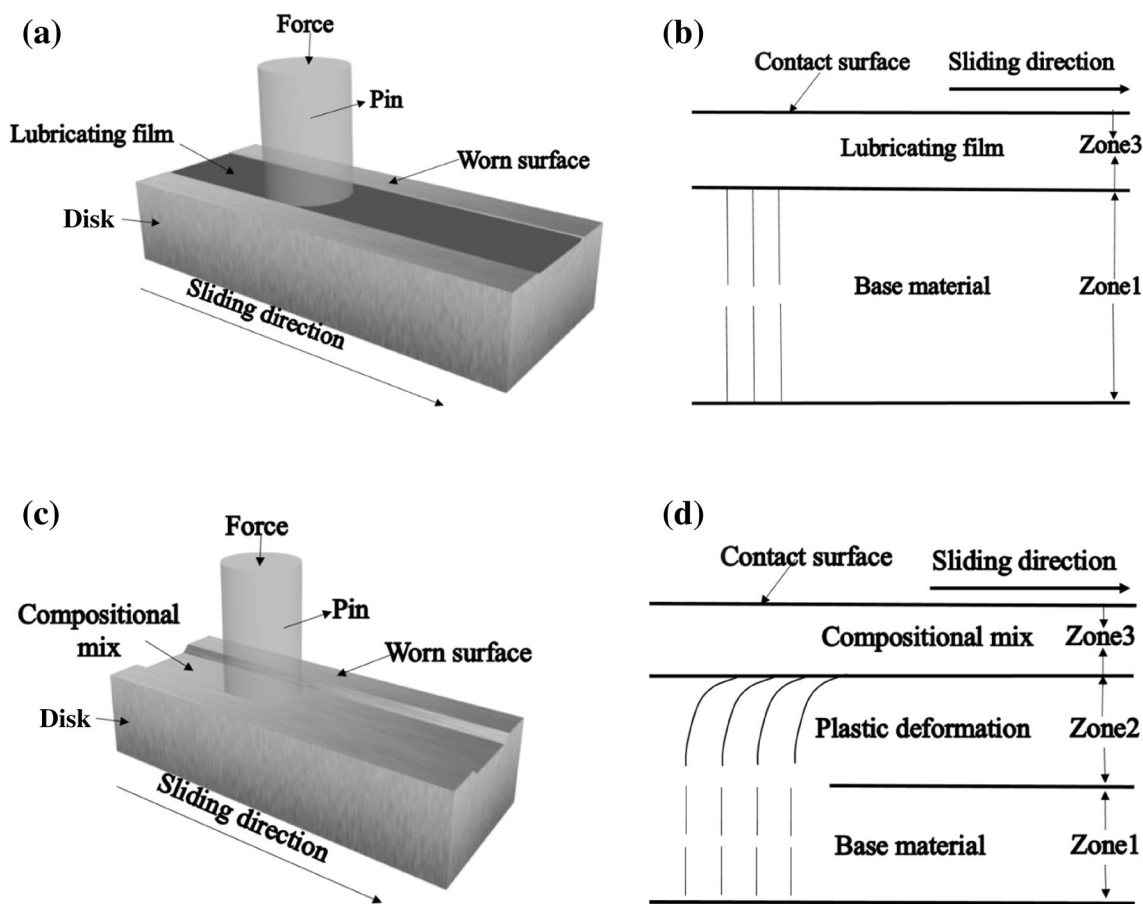


Fig. 12 Schematic illustration of wear mechanism. **a** Sliding process with lubricating film; **b** cross section with formed lubricating film; **c** sliding process without lubricating film; **d** cross section without lubricating film

wear loss. The functions of the lubricating film could be summarized as follows: On the one hand, the lubricating film can prevent direct contact of the surfaces of the tribopair materials. On the other hand, it can reduce the shear strength of the contacting thin layer. As a result, the friction coefficient was significantly reduced. When the amount of MLG/Fe₂O₃ addition fell below or above the critical value, the lubricating film was not formed on the surface (Fig. 12c), and the frictional properties of TMCs were worse than those with a lubricating film. Moreover, the area underneath TMCs surface underwent a severe plastic deformation (Fig. 12d), indicating that there was no protection provided by MLG/Fe₂O₃ (1:2) nanocomposites. The characteristic and formation of the lubricating film on the surfaces of tribopair material are believed to be the predominant parts of the wear mechanism.

4.3 Structure of lubricating film

The structure of the lubricating film is schematically shown in Fig. 13. As we know, graphene is a two-dimensional

material, presenting unique friction and wear properties (not typically seen in conventional materials), which is totally due to its lamellar structure (as shown in Fig. 13). Multilayer graphene possesses similar properties to graphene, and in

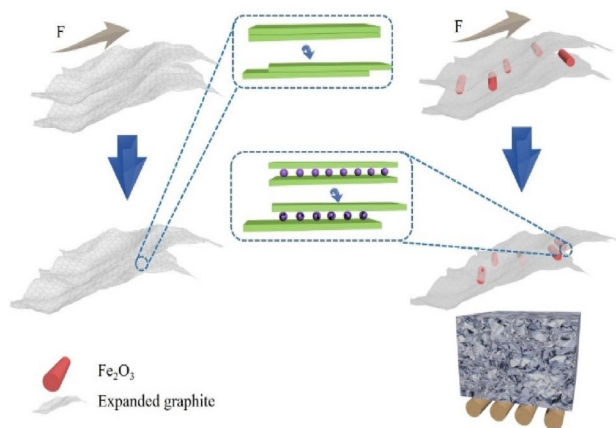


Fig. 13 Schematic illustration of structure of lubricating film

order to illustrate the structure of the lubricating film clearly, the structure of MLG was needed to introduce in Fig. 13 as well. During sliding, MLG would be adsorbed onto the worn surface and the surface of wear debris, and its theoretical function is dependent on the movement of graphene layers. During this process, MLG possessed a low shear force, resulting in a lubricating function and a low frictional coefficient. In our present work, spindle-shaped Fe_2O_3 particles are vaguely shown in Fig. 3b. Thereby, a red bar is drawn in Fig. 13 to represent the structure of Fe_2O_3 particles.

Since the spindle-shaped Fe_2O_3 particles were randomly distributed on the surface of MLG (Fig. 4c), it could be speculated that the structure of MLG/ Fe_2O_3 (1:2) nanocomposites unit was similar to a rolling wood structure, which is closely related to the structure of the lubricating film. When MLG/ Fe_2O_3 nanocomposites were supplied onto the sliding interface, both the adsorption of MLG and the sintering of Fe_2O_3 are related to the formation of the lubricating film. According to the order from small to large size, MLG in the composites preferred to be adsorbed to the surface. Subsequently, the nomadic Fe_2O_3 particles and those distributed on the surface of small-sized composites were also sintered on MLG layer due to the high surface energy. Under the combined effect of pressure (caused by the normal force), temperature (cause by friction heat), and an appropriate amount of MLG/ Fe_2O_3 addition, the formation of the lubricating film was initiated. The lubricating film was compacted every sliding cycle, and finally, a protective lubricating film was formed, whose structure was similar to a rolling wood as shown in Fig. 13.

5 Conclusions

1. The tribological properties of TMCs can be improved with the addition of MLG/nano- Fe_2O_3 composites, and a significant decrease in the friction coefficient was obtained, reducing this parameter up to 50%.
2. There was a range of critical value of MLG/ Fe_2O_3 addition, which made TMCs undergo a transition of severe wear to mild wear.
3. The well-protected effect induced by MLG/nano- Fe_2O_3 composites was attributed to the formation of a protective lubricating film, which prevented the surface from coming in direct contact, resulting in improved tribological performance.

4. The lubricating film was 15–20 μm thick and made up of MLG/ Fe_2O_3 (1:2) nanocomposites. Its structure was speculated to be similar to a rolling wood.

Acknowledgements The authors would like to acknowledge the financial support of this work by National Natural Science Foundation of China (No. 51505199) and Postgraduate Research & Practice Innovation Program of Jiangsu Province (KYCX19_1670).

References

- [1] J.X. Zhang, Z.Z. Zhuang, Y.T. Jiao, H.X. Yang, Y.Q. Li, J. Zhang, P. Gao, *J. Power Sources* 419 (2019) 99–105.
- [2] H. Zhou, J. Zhang, J. Zhang, X.F. Yan, X.P. Shen, A.H. Yuan, *Inorg. Chem. Commun.* 54 (2015) 54–56.
- [3] J.X. Shao, H. Zhou, J.H. Feng, M.Z. Zhu, A.H. Yuan, *J. Alloy. Compd.* 784 (2019) 869–876.
- [4] H. Zhou, X.Q. Liu, J. Zhang, X.F. Yan, Y.J. Liu, A.H. Yuan, *Int. J. Hydrog. Energy* 39 (2014) 2160–2167.
- [5] C. Lee, X. Wei, J.W. Kysar, J. Hone, *Science* 321 (2008) 385–388.
- [6] K.I. Bolotin, K.J. Sikes, Z. Jiang, M. Klima, G. Fudenberg, J. Hone, P. Kim, H.L. Stormer, *Solid State Commun.* 146 (2008) 351–355.
- [7] A.A. Balandin, S. Ghosh, W. Bao, I. Calizo, D. Teweldebrhan, F. Miao, C.N. Lau, *Nano Lett.* 8 (2008) 902–907.
- [8] W.Z. Zhai, X.L. Shi, J. Yao, A.M.M. Ibrahim, Z.S. Xu, Q.S. Zhu, Y.C. Xiao, L. Chen, Q.X. Zhang, *Compos. Part. B* 70 (2015) 149–155.
- [9] Z.S. Xu, X.L. Shi, W.Z. Zhai, J. Yao, S.Y. Song, Q.X. Zhang, *Carbon* 67 (2014) 168–177.
- [10] C.F. Gutierrez-Gonzalez, A. Smirnov, A. Centeno, A. Fernández, B. Alonso, V.G. Rocha, R. Torrecillas, A. Zurutuza, J.F. Bartolome, *Ceram. Int.* 41 (2015) 7434–7438.
- [11] S.S. Kandanur, M.A. Rafiee, F. Yavari, M. Schrameyer, Z.Z. Yu, T.A. Blanchet, N. Koratkar, *Carbon* 50 (2012) 3178–3183.
- [12] H. Wang, G.Y. Xie, Z.G. Zhu, Z. Ying, Y. Zeng, *Compos. Part. A* 67 (2014) 268–273.
- [13] D. Berman, A. Erdemir, A.V. Sumant, *Carbon* 59 (2013) 167–175.
- [14] D. Berman, A. Erdemir, A.V. Sumant, *Carbon* 54 (2013) 454–459.
- [15] H. Kato, *Tribol. Int.* 41 (2008) 735–742.
- [16] H. Kato, *Wear* 255 (2003) 426–429.
- [17] H. Kato, K. Komai, *Wear* 262 (2007) 36–41.
- [18] A. Iwabuchi, H. Kubosawa, K. Hori, *Wear* 139 (1990) 319–333.
- [19] Y. Zhou, S.Q. Wang, W. Chen, *Metall. Mater. Trans. A* 48 (2017) 3287–3299.
- [20] A.C. Ferrari, J.C. Meyer, V. Scardaci, C. Casiraghi, M. Lazzeri, F. Mauri, S. Piscanec, D. Jiang, K.S. Novoselov, S. Roth, *Phys. Rev. Lett.* 97 (2006) 187401.
- [21] W. Ames, A.T. Alpas, *Metall. Mater. Trans. A* 26 (1995) 85–98.